Dynamics Monitoring and Disaster Assessment for Watershed Management Using Time-Series Satellite Images

4 authors, including:

Jiann-Yeou Rau
National Cheng Kung University
78 PUBLICATIONS   **1,084** CITATIONS

SEE PROFILE

L. Y. Chen
National Chiao Tung University
90 PUBLICATIONS   **1,096** CITATIONS

SEE PROFILE

Jin-King Liu
LIDAR Technology Co., Ltd.
73 PUBLICATIONS   **636** CITATIONS

SEE PROFILE

Dynamics Monitoring and Disaster Assessment for Watershed Management Using Time-Series Satellite Images

Jiann-Yeou Rau, Liang-Chien Chen, Jin-King Liu, and Tong-Hsiung Wu

Abstract—**This paper presents a mechanism that utilizes intensive multitemporal and multisensor satellite images to monitor land cover dynamics. The proposed approach could be applied for regular dynamics monitoring, disaster monitoring and assessment, and vegetation recovery after natural disasters. The disaster monitoring and assessment are the most important issues imbedded in the program. This paper gives an example using the proposed mechanism to cover a major watershed in Taiwan. Often natural hazards such as typhoons or earthquakes trigger landslides or debris flows, which can deliver large amounts of sediment into a reservoir, decreasing its capacity for water storage. Disaster assessment prior to decision-making and support efforts is a must. Three major typhoons that happened in 2004 and 2005 will be discussed here. The proposed mechanism is demonstrated to be feasible, practical, and effective, since with it we are able to generate disaster assessment in a shorter time than with on-site or aerial-photo surveying alone provided that intensive satellite images are available.**

Index Terms—**Disaster assessment, disaster monitoring, remote sensing.**

I. INTRODUCTION

THE MOST important work of a water-resource agency is reservoir management. It includes the protection of the environment and the water quality of the water sources and prevention of water pollution. In addition to man-made problems, natural hazards such as typhoons or earthquakes may trigger landslides or debris flows, which deliver large amounts of sediment into a reservoir, decreasing its capacity for water storage. This makes disaster assessment a must for decision-making and support. It is thus crucial to provide a land-cover dynamics and disaster assessment report which can be done by means of remote sensing and geographic information system (GIS) techniques, to fulfill the requirements of reservoir management.

J.-Y. Rau and L.-C. Chen are with the Center for Space and Remote Sensing Research, National Central University (NCU), Jhong-Li 320, Taiwan, R.O.C. (e-mail: jyrau@csrsr.ncu.edu.tw; lcchen@csrsr.ncu.edu.tw).

J.-K. Liu is with the Energy and Environment Laboratory, Industrial Technology Research Institute, Hsin-Chu 310, Taiwan, R.O.C. (e-mail: jkliu@itri.org.tw).

T.-H. Wu is with the North Region Wate Resource Office, Lung-Tan 325, Taiwan, R.O.C. (e-mail: f20@wranb.gov.tw).

In this paper, we propose a mechanism to monitor the dynamics of a watershed that integrates intensive satellite images and GIS technology to facilitate disaster assessment and to support decision-making and rehabilitation.

We demonstrate an example of dynamics monitoring for the Shihmen Reservoir watershed. This reservoir is managed by the North Region Water Resource Office (NRWRO), Water Resource Agency, Taiwan. The Shihmen Reservoir is one of the largest and most important reservoirs in northern Taiwan. It supplies water to some two million people in the area and supports the high-tech industry, as well as a well-developed agricultural area. The watershed covers an area of 763.4 km^2 and has a 3000-m terrain variation.

From the perspective of geology, the island of Taiwan is in a relatively new mountain-building belt. The natural rock bodies are highly fractured with numerous joints and cleavages. The majority of the area is covered with Oligocene and Miocene argillites and shale, which are soft and fragile, particularly when saturated with moisture. This means that the landslides are easily induced by rainfall and earthquake [1], [2]. The Chi-Chi earthquake (also known as the 921 earthquake) occurred on September 21, 1999, in central Taiwan and measured 7.3 on the Richter scale [3]. The Chi-Chi earthquake triggered more than 20 000 landslides on the island. Due to the coseismic weakening of the substrate material, this increased the danger of landslides after a typhoon [4]. Although the epicenter was located around 85 km south of the Shihmen Reservoir at 8.0 km in depth, the influence of the Chi-Chi earthquake still remained at around 4–5 in intensity [3]. The coseismic landslide intensity is correlated with the earthquake magnitude [5], [6]. After an earthquake, coseismic landslide debris is flushed from the catchment's area [7], [8] as well seismically weakened rock mass may be removed from hilltops whenever cumulative rainfall is sufficient. This geological instability makes the monitoring of landslides an important part of disaster management.

In order to protect the reservoir, near real-time monitoring of the watershed is necessary. A long-term project employing intensive multitemporal and multisensor satellite images to monitor the Shihmen Reservoir dynamics has been initiated. It is to be conducted by the NRWRO collaboration with the Center for Space and Remote Sensing Research (CSRSR) of National Central University. The first phase of the project runs from 2003 to 2007. SPOT and FORMOSAT-2 satellite images with high acquisition frequency are utilized to monitor the dynamics of the watershed. The dynamics can be categorized

into three types, human-related activities, natural hazards, and vegetation recovery after a disaster. Human-related activities include farming, construction, logging, cultivation, tourism, and so on. Two types of disasters are included, namely explicit and implicit. The explicit ones include forest fire and typhoons. In which, typhoons induce landslides and debris flows. The implicit disaster is the earthquake, which occurred five years before the reported typhoons what have been observed is the long-term influence of the earthquake.

For regular dynamics monitoring, orthorectification is applied to each cloud-free satellite image. Automatic land-cover change detection can be proceeding. Once a conspicuous change has been detected, the area is subject to on-site inspection and a report with suggestions to prevent further deterioration or pollution is made.

In case of disasters, an emergency daily data acquisition plan will be launched. The disaster assessment report is performed using GIS techniques. In this paper, we discuss three major typhoons, i.e., Typhoon AERE, Typhoon MASA and Typhoon TALIM, that occurred in the summers of 2004 and 2005 as an illustration. The regular monitoring of land cover dynamics might be considered as an important part in preventive mitigation for hazards. On the other hand, the role of the monitoring switches to assessment for natural disasters after the events.

In addition, we also monitor the vegetation recovery process using a procedure similar to regular dynamics monitoring. Due to the steep terrain in the watershed, most of the landslides are unreachable, so, man-made reconstruction is difficult. Here, we compare the efficiency of a man-made reconstruction process with that of the natural recovery. This comparison can be used for decision-making in reservoir management.

II. METHODOLOGY

The workflow of the process is divided into six major steps, namely: 1) the data acquisition plan; 2) rigorous orthorectification; 3) land cover change detection; 4) *in situ* inspection and reporting; 5) disaster assessment; and 6) vegetation recovery monitoring.

A. Data Acquisition Plan

FORMOSAT-2 was designed by the National Space Organization (NSPO). It is the Taiwan's first resource satellite. It was successfully launched on May 21, 2004. It has a unique daily revisit capability with one panchromatic band (PAN) and four multispectral bands (R, G, B, N-IR) with 2- and 8-m spatial resolutions, respectively [9]. Fig. 1 illustrates data acquisition plan of FORMOSAT-2. Due to its 24-km swath width, the island of Taiwan had to be segmented into seven strips. In Fig. 1, the location of the Shihmen Reservoir watershed is marked by a box. We utilized both FORMOSAT-2 and SPOT images for dynamics monitoring. The data acquisition plan can be categorized into two phases, i.e., regular monitoring and disaster event.

For regular monitoring, about two images of the watershed area can be acquired every three days. A cloud-free image with less than 50% cloud cover is chosen as candidates for
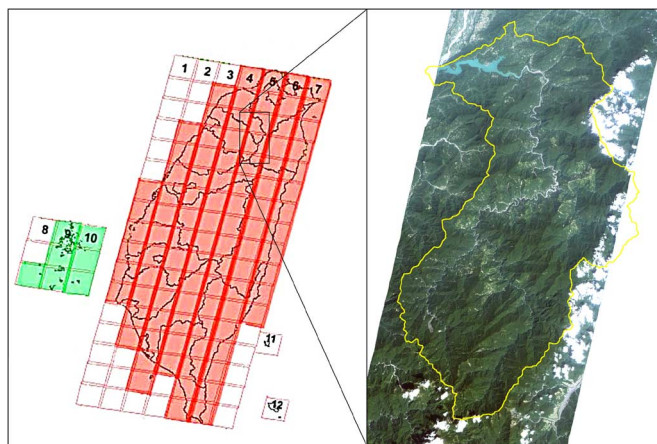

Fig. 1. Data acquisition plan of FORMOSAT-2 satellite and location of the Shihmen Reservoir watershed.

land cover change detection. The time-interval between the two consecutive datasets selected should be at least two weeks.

Once a disaster event, such as a typhoon or an earthquake, it may introduce natural hazards, an emergency response mechanism is initiated. The responsibility for the initiation and termination of the mechanism is made by the CSRSR to incorporate with NSPO and SPOT Image, Inc. Daily data acquisition is targeted under such a mechanism.

B. Rigorous Orthorectification

For the purpose of change detection, georeferencing between datasets is a must. The orthoimages used in this project were generated by the multisensor geocoded production system (MSGPS) [10]. The MSGPS system utilizes ground control points and a rigorous sensor model for orbit adjustment, followed by least-squares filtering [11]. A digital terrain model is used for terrain relief correction. Images taken on different dates are rectified and projected onto the same map projection system for further overlay analysis.

C. Land Cover Change Detection

We combine the change vector analysis (CVA) [12] and normalized difference vegetation index (NDVI) [13], [14] to detect land cover changes. CVA is a band transformation method used to calculate the magnitude of variation between multispectral and multitemporal change vectors. NDVI provides the standard index for comparing the vegetation chlorophyll using satellite images. It can also be used as an indicator of relative biomass and greenness [15], [16].

A higher NDVI indicates higher levels of healthy vegetation. In this paper, it is assumed that alteration in land-use causes a change in the land-cover. This means that the relative spectral value or greenness will be changed resulting in a certain degree of difference in the CVA or NDVI. However, in the case where land cover changes from bare soil to buildings, the NDVI difference is insignificant, and will be considered as "not changed." In this case, the CVA magnitude may be examined. On the other hand, a change in land cover from vegetation to

bare soil induces a more significant reduction in the NDVI than in the CVA magnitude. That is why in the project we adopt both methods to improve the reliability.

An empirical threshold for the automatic change detection step is selected. When changes exceed the threshold, the detected location will be vectorized for further analysis. In case of NDVI method, the empirical threshold for the NDVI difference is set as 0.3. The threshold is adjusted and verified after long-term correspondence between the change detection results and *in situ* inspections. In order to assure the quality of the detection results and avoid clouds or shadows, manual editing is employed.

D. In Situ Inspection and Reporting

Due to the limits of the spatial resolution of the SPOT and FORMOSAT-2 satellite images, it is impossible to distinguish subtle ground truth. It is also necessary to determine whether land cover change is due to legal or illegal causes. Thus, a group of three patrolmen perform *in situ* inspections. If any land cover change is detected, they must perform timely on-site survey. If illegal land use is found, the land owner will be prosecuted so as to avoid further land deterioration. However, in the Shihmen watershed the height variation can be as much as 3000 m. The steepness of the terrain sometimes makes a detailed inspection impossible. In cases of disaster, a helicopter is used for aerial inspection, which is efficient but is too costly for normal situations.

E. Disaster Assessment

Another important goal of this project is the assessment of disaster damage. That is, when a typhoon, forest fire, or earthquake occurs in the watershed, a damage assessment report has to be provided within one week in case a cloud-free satellite image is acquired. Since the geographic distribution of the damaged areas is crucial for decision-making, the damage assessment report must include the location, area, and terrain slope of these areas.

The U.S. Geological Survey [17] describes landslide types and processes. There are more than 22 factors that could introduce landslides. As described in the introduction, the Chi-Chi earthquake was a key factor in inducing landslides that were later triggering by heavy rainfall. Thus, in the case of a disaster, both rain-fall distribution and geological formation must be used to analyze possible reasons behind the disaster. Additionally, human-activities are also possible factors that can induce landslides, so their impact has to be further analyzed utilizing the land-use information.

F. Vegetation Recovery Monitoring

The objective of this task is to compare the speed between man-made reconstruction and natural recovery of vegetation. For the man-made reconstruction, we monitored an old land-slide site. For natural recovery monitoring, we focused on landslide areas triggered by Typhoon AERE. An automatic monitoring procedure, similar to that for land-cover change

TABLE I
STATISTICS OF DETECTED DYNAMICS

Category	Number of Places	Percentage of Total Number (%)	Area (Hectares)	Percentage of Total Area (%)
Un-reachable	133	29.09	94.96	13.83
Logging	29	4.61	18.49	2.69
Cultivation	187	29.73	135.24	19.70
Construction	33	5.25	18.66	2.72
Forest Fires	1	0.16	2.14	0.31
Landslides	246	31.16	416.99	60.74
Total	629	100.00	686.48	100.00

detection, was adopted. In contrast to change detection, we only checked NDVI increments. The NDVI threshold for successful vegetation recovery is set at 0.3, too.

III. ACHIEVEMENTS

Three major achievements: 1) regular dynamics monitoring; 2) disaster assessment; and 3) the monitoring of vegetation recovery are discussed.

A. Regular Dynamics Monitoring

In this section, we summarize the statistics of dynamics monitoring from May of 2003 to November of 2005, a total of 946 days. During this period 436 images were acquired. This means that the average temporal resolution for data acquisition is 0.46 images per day. This intensive image acquisition rate over a specific area could be the highest one ever reported. In which, 59 images were chosen for land-cover change detection and disaster assessment. Due to weather conditions and the two-week criteria, the temporal resolution for change detection is about 19 days, i.e., less than three weeks. The satellite images used included SPOT-2, SPOT-4, SPOT-5, and FORMOSAT-2 images. In total, we detected 629 changes with a total area of 686.48 ha. Among those changes, 496 places were on-site or helicopter inspected. Due to steep terrain, sometimes foot patrols were impossible, so there were 133 places are classified as unreachable.

Table I divides the dynamics into six classes. "Forest fires" occur due to uncertain reasons. "Landslides" were induced by the typhoons or heavy rainfall. The others were all due to human activities, such as logging, cultivation, or construction. In Table I, we notice that the largest dynamics sections of the watershed belong to the "Un-reachable," "Cultivation," and "Landslide" classes. The "Logging" class is mostly due to bamboo cultivation. When this is combined with the "Cultivation" class, we found that agriculture activity in the watershed was intense. During this period, nine illegal instances of activities were detected, covering a total area of 5.7 ha. These illegalities were reported to the government for prosecution so as to prevent further deterioration or pollution. The described achievements are encouraging and demonstrate the applicability of the proposed mechanism.
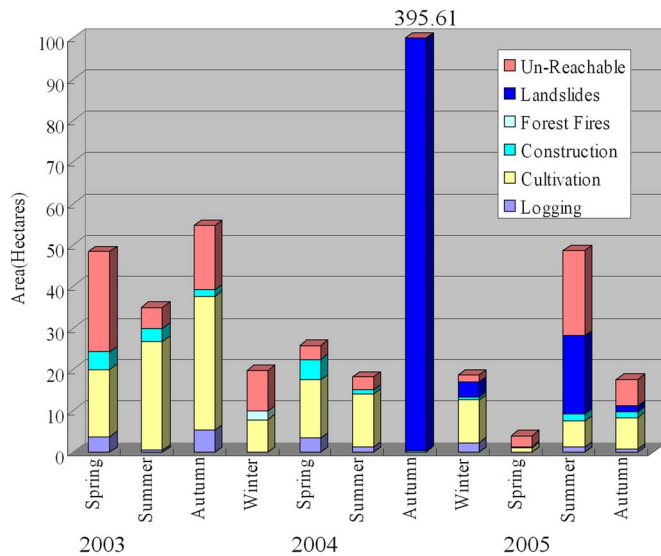
Fig. 2. Seasonal dynamics changes in the watershed. Spring (March–May). Summer (June–August). Autumn (September–November). Winter (December–February).

Fig. 3. Four typical landslides induced by Typhoon AERE. The lower right photo shows the largest landslide in Fig. 4(b) taken from the west.

TABLE II
GENERAL STATISTICS FOR THE THREE TYPHOONS

Name of Typhoon	AERE	MASA	TALIM
Dates	Aug. 23-25, 2004.	Aug.4-5, 2005	Aug. 31, 2005
Max. Cumulative Rainfall	1,607 mm	1,273 mm	533 mm
Total Area of the Landslides	393 hectare	34 hectare	3 hectare
No. of Damaged Places	222	33	15

In summary, Fig. 2 illustrates seasonal dynamics changes in the Shihmen Reservoir watershed. We note that the maximum variation was due to Typhoon AERE which occurred in the autumn of 2004. Aside from typhoon-induced landslides, seasonal changes are mostly due to agricultural activities carried out by aboriginal inhabitants.

B. Disaster Assessment

From the location, terrain slope, and spectral response of the satellite images, we can deduce that most of the land-cover change in the "Un-reachable" class was due to landslides. In addition to confirmed landslides, the "Landslide" class includes about two-thirds, i.e., 13.83 plus 60.74, of all the detected dynamics. This indicates the importance of disaster monitoring in the watershed.

During the period of regular monitoring, several typhoons impacted the watershed. The minor typhoons have not been singled out. Three major one are chosen as targets, i.e., Typhoon AERE, Typhoon MASA, and Typhoon TALIM. In this section,
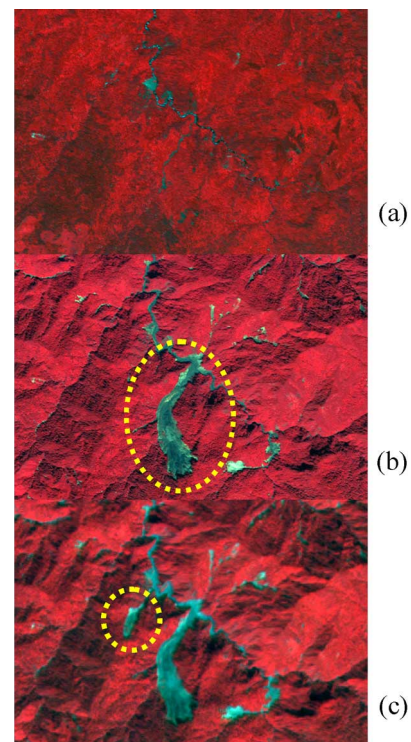

Fig. 4. SPOT Images acquired before and after the two typhoons. (a) SPOT-5, August 16, 2004, (b) SPOT-5, October 12, 2004, and (c) SPOT-2, October 14, 2005.

some general statistics describing the three typhoons will be given. Since Typhoon AERE was the most serious one that ever occurred in this watershed, we will further analyze some of the factors that trigger the landslides, such as the hydrology, geology and land-use.

Table II gives general statistics about these dynamics. In total, there were about 270 landslides covering a total area of 430 ha. This area included more than one-half of all dynamics detected during the project, i.e., 686.48 ha. Four typical landslides induced by Typhoon AERE are pictured in Fig. 3. Fig. 4 illustrates three SPOT satellite images acquired
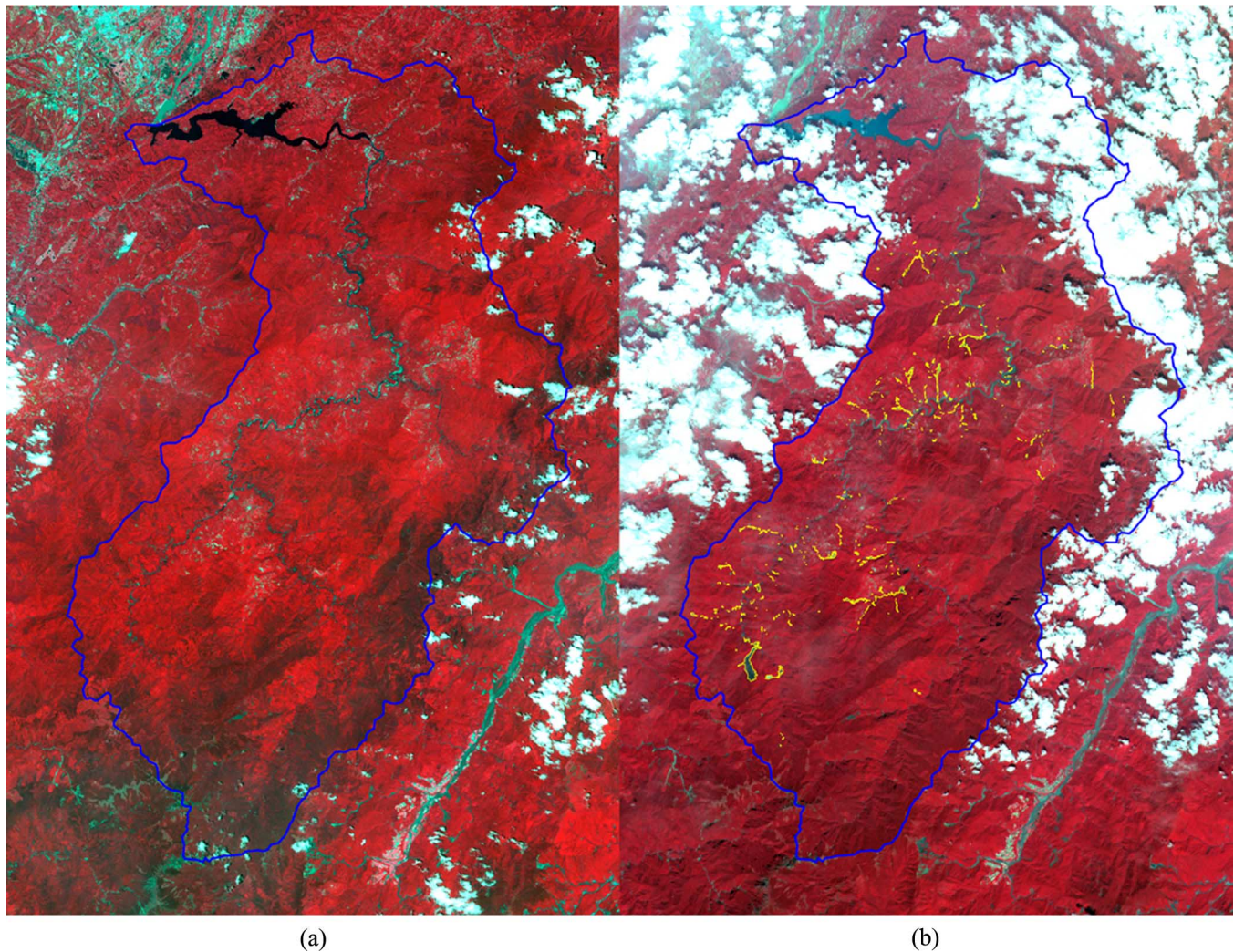
Fig. 5.   SPOT images acquired (a) before (Aug. 16, 2004) and (b) after (Sep. 19, 2004) Typhoon AERE.

before Typhoon AERE (August 16, 2004), between Typhoon AERE and Typhoon MASA (October 12, 2004), and after Typhoon MASA (October 14, 2005). Fig. 4 depicts the largest landslide induced by Typhoon AERE with an area of 77.7 ha, as shown by the dotted circle in Fig. 4(b). A close-up photograph taken from a helicopter is shown in the lower right photo of Fig. 3. From Fig. 4(c), one may notice that another landslide was induced by Typhoon MASA in the neighborhood, denoted by the dotted circle in Fig. 4(c).

1) General Statistics: From Table II, we can see that among the others, Typhoon AERE was the most serious one. According to the National Fire Agency, Ministry of Interior, Taiwan, Typhoon AERE caused 14 deaths, 15 people were missing, and 399 people injured. In addition, 72 buildings were completely destroyed and 44 buildings severely damaged throughout the country [18]. The power supply for more than 20 000 buildings failed and the water supply in the area was too turbid to use for more than two weeks. Fig. 5 shows the SPOT images taken before [Fig. 5(a)] and after [Fig. 5(b)] Typhoon AERE. The detected landslides are overlaid on the image taken after typhoon.

After the typhoon, some major transportation channels were blocked due to the destruction of bridges and roads by debris flows and landslides. Comprehensive damage assessment and geographical analysis were difficult to obtain in a short time with the traditional approach. We thus initiated an emergency satellite image acquisition program. Although more than one image could be acquired every day, due to the heavy cloud cover, several images had to be integrated for disaster assessment.

2) Disaster Assessment for Typhoon AERE: Since the adopted mechanism is based on geospatial data analysis, we may analyze some of the factors that caused landslides after Typhoon AERE. Fig. 6 illustrates the rainfall isolines superimposed over the landslides introduced by Typhoon AERE. The isolines were interpolated by the inverse distance-weighting method from precipitation data collected at ten hydrological stations, depicted in Fig. 6 with the square boxes. We can see that the contour values gradually changed from 600 to 1600 mm from east to west in the watershed. We note that most landslides occurred at areas with 800 to 1600 mm of cumulative rainfall.
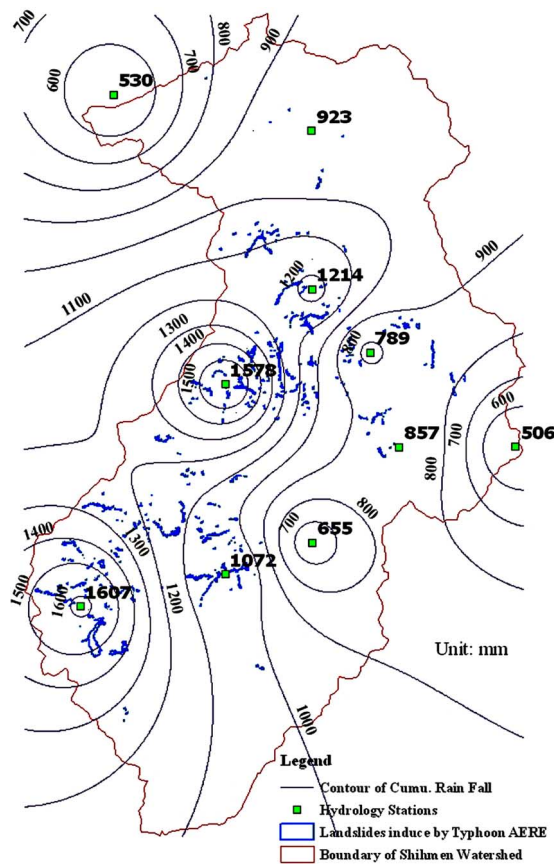
Fig. 6. Cumulative rainfall isolines overlaid by landslides induced by Typhoon AERE.

TABLE III
LANDSLIDES IN VARIOUS ROCKTYPES

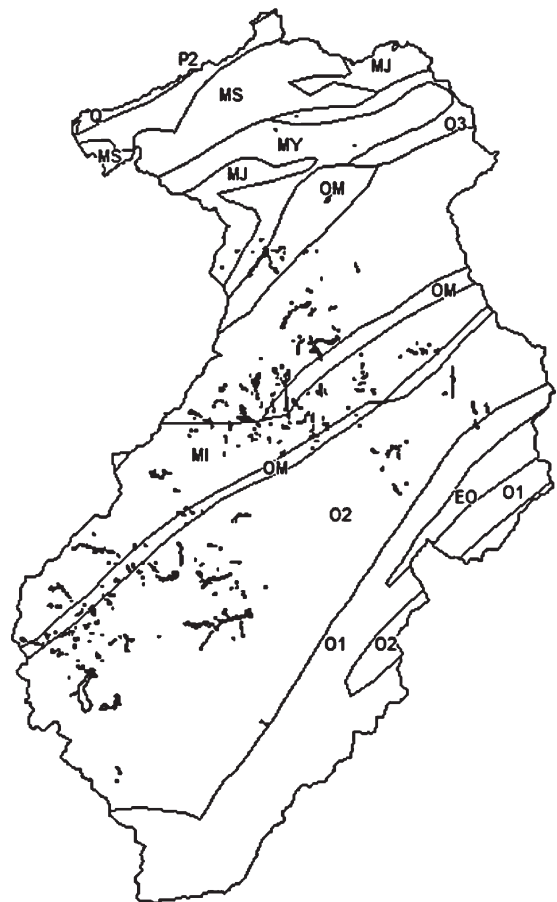| Rock Type	Lithologic Description	Rocktype Areas (Hectares)	Slide Areas (Hectares)	*SlideAreaRatio x 10⁴	Slide Area Percentage (%)
Q	Alluvium	301.30	0.00	0.00	0.00
P2	Sandstone, mudstone, shale	0.00	0.00	0.00	0.00
MS	Sandstone, shale	3,957.30	0.00	0.00	0.00
MJ	Sandstone, shale	3,699.92	1.18	3.14	0.30
MY	Sandstone, shale	3,905.25	3.65	9.21	0.93
MI	Argillite slate phyllite sandstone interbeds	8,548.99	68.19	78.57	17.35
OM	Sandstone shale, coaly shale	5,192.93	34.54	65.51	8.79
O3	Sandstone shale	1,421.02	0.18	1.25	0.05
O2	Argillite, indurated sandstone	36,701.68	285.21	76.55	72.56
O1	Quartzitic sandstone, slate, graphitic shale	11,471.21	0.14	0.12	0.04
EO	Slate,phyllite,with sandstone interbeds	1283.63	0.00	0.00	0.00

*SlideAreaRatio = Slide Areas / Rocktype Areas

Table III outlines the 11 geological types in the watershed [1], [2] and landslides in relation to the various rock types. In Fig. 7, the landslides induced by Typhoon AERE are overlaid with the geological formations. The coseismic effect of the Chi-Chi earthquake caused the substrate material to weaken. Thus, together with the heavy rainfall due to Typhoon AERE, a substantial number of landslides took place in the argillite and shale-type terrains, which includes the lithologic types designated as O2, OM, and MI. From Table III, it can be seen that MI, OM, and O2 have higher "SlideAreaRatio" than other rock types. We thus realize that landslides may happen more easily in argillite and shale-type terrains.

Fig. 8 depicts land-use distribution in the watershed. The road systems were expanded from each road polyline into a buffer-zone 100 m in width. Fig. 9 gives statistics for land-use type in the landslide areas. To analyze the relationship between landslides and human activities, we categorized all land-use type into natural land and human-related classes. It is found that 88.3% of all landslide areas, are located in the natural land class, which includes river, bare soil, mixed forest, bamboo, conifers, grass, broadleaf trees, and conifer-broadleaf trees. The remaining part, i.e., 11.7%, are in areas related to human-related activities such as road systems, shrubs, rice, cutting areas, and unirrigated farmland. Since the causal relationship between landslides

Fig. 7. Landslides in relation to various geologic formations.

Legend (Fig. 8):
- 🔴 Mixed-Forest
- ◍ Bamboo
- ⚫ Conifer Tree
- 🟣 Unirrigated Farmland
- 🟡 Grass Land
- 🔴 Broadleaf Tree
- 🟣 Shrub
- 🟠 Building
- ◍ Cutting Area
- Mixed Conifer-Broadleaf Tree
- Fruit Farm
- ⚫ Rice
- 🟠 Tea
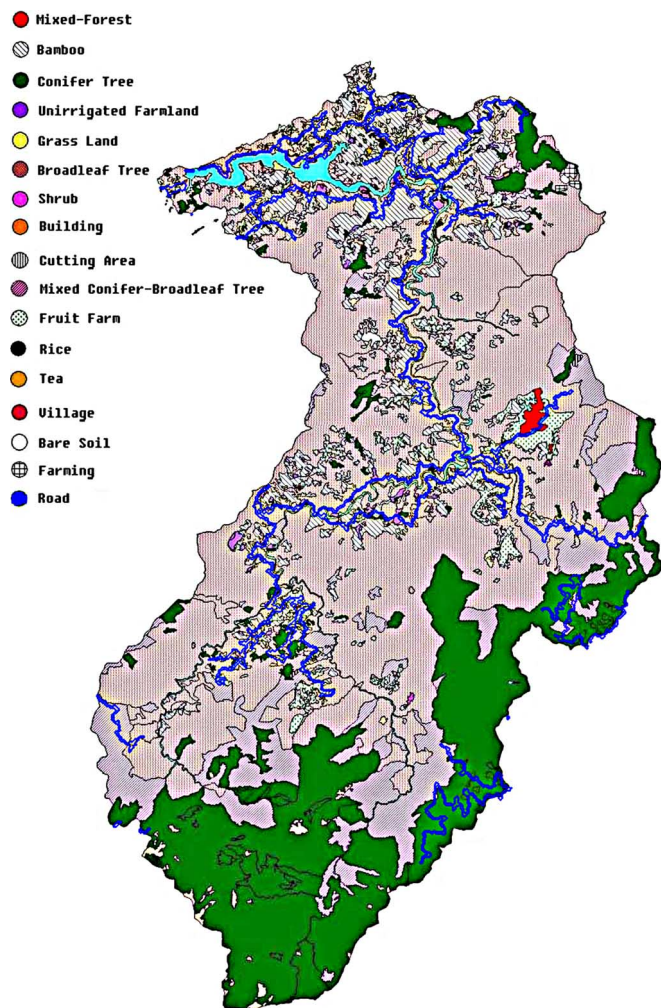- 🔴 Village
- ⚪ Bare Soil
- ⊕ Farming
- 🔵 Road

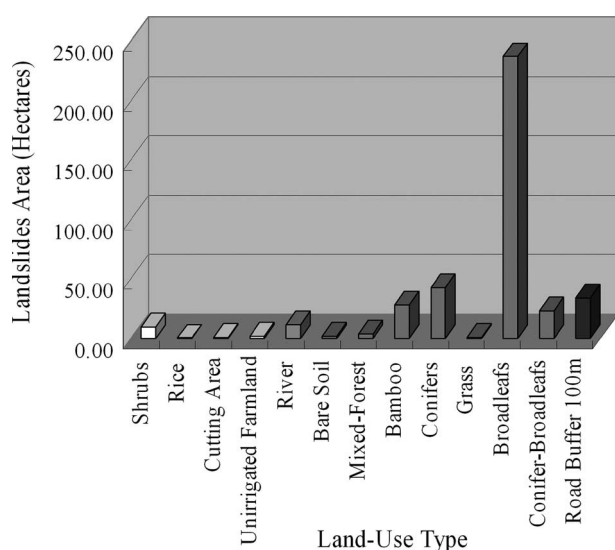Fig. 8. Land-use distribution in the watershed.

Fig. 9. Landslide area and land-use type.

and road systems is not fully understood, we counted all slide areas that are related to road systems as a man-made contribution.
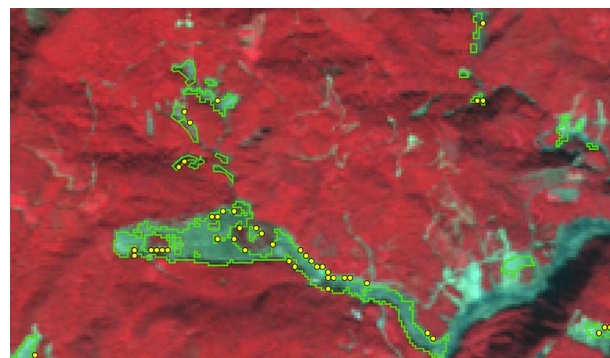

Fig. 10. Example of natural recovery monitoring. The green polygons denote the boundary of landslides induced by Typhoon AERE. The yellow dots depict the detected vegetation recovery.

The reason why the landslide occurred on the river class is because the terrain is steep beside the river and some landslides occurred close to the river. Additionally, due to the satellite imagery has a resolution around 8 to 20 m, while the land cover is vector coverage, after overlay analysis a river class may contain a considerable number of landslides.

3) Monitoring of Vegetation Recovery: A SPOT-5 image acquired on October 12, 2004, after Typhoon AERE is used as the reference image. Two comparisons are made with two images acquired about seven months (March 16, 2005) and 13 months (October 14, 2005) after Typhoon AERE. We detected 178 and 58 vegetation recovered pixels in these two compared images, respectively. Fig. 10 illustrates an example of successful natural recovered areas marked by yellow dots. Each pixel represents an area of 100 m^2. Thus, the recovered areas cover 1.78 and 0.58 ha during the two periods. The reason that the vegetation recovery was reduced from 1.78 to 0.58 ha is because of Typhoon TALIM. From Fig. 10, we can see that the natural recovered pixels are randomly distributed and without significant structure. This monitoring of a natural recovery process shows that recovery efficiency was low, even one year after the typhoon.

On the other hand, we also monitored the man-made vegetation reconstruction of an old landslide located at Xiu-Luan. Fig. 11 shows three SPOT images acquired on October 12, 2004, April 30, 2005, and October 14, 2005, respectively, in which the blue polygons denote the landslides induced by Typhoon AERE, and the yellow dotted polygons indicate the reconstruction area within the Xiu-Luan landslide. Fig. 11(a), (b), and (c) shows the area before the man-made reconstruction commended, in the middle of the vegetation recovery process, and the final result, respectively. We can compare the two close-up photographs taken on January 19, 2005, i.e., Fig. 12(a), the first day of man-made reconstruction, and April 1, 2005, i.e., Fig. 12(b), that grass have commenced to grow on the landslide. From Fig. 11(b) and (c), we can detect significant vegetation recovery.

From the above comparison, we realize that man-made reconstruction is more efficient than the natural recovery process. However, since the Xiu-Luan landslide was close to a residential area, so man-made reconstruction was easy. For unreachable landslides, man-made reconstruction would be difficult
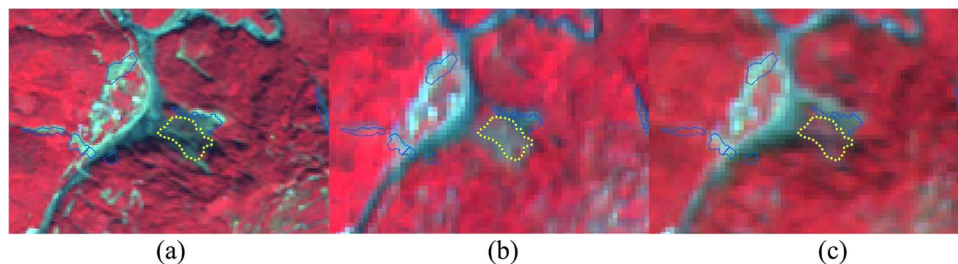
Fig. 11. Satellite images used for monitoring the man-made reconstruction process at the Xiu-Luan landslide. The blue polygons denote the boundary of landslides induced by Typhoon AERE. Yellow-dotted polygons indicate the reconstruction area. (a) SPOT-5, October 12, 2004, (b) SPOT-2, April 30, 2005, and (c) SPOT-2, October 14, 2005.

and costly. There may have to be a tradeoff made for the management of the reservoir.

IV. CONCLUSION

We have proposed a mechanism that uses multitemporal and multisensor satellite images to monitor the dynamics of a watershed for the purpose of disaster monitoring and assessment. A threefold monitoring process is discussed in this paper using the Shihmen Reservoir watershed as an example.

A. Regular Dynamics Monitoring

For regular dynamics monitoring, the data acquisition frequency of the proposed scheme is high enough to make the monitoring in near real-time possible. The temporal resolution for data acquisition is on the average about one image every two days. For land-cover change detection, the temporal resolution can be less than three weeks. By means of automatic change detection techniques and *in situ* inspection, the dynamics of the watershed can be effectively monitored. In the project (about 1000 days) we detected 629 places where dynamic changes occurred covering a total area of 686.48 ha. In which, nine illegal instances of activities were detected, with a total area of 5.7 ha. In summary, the landslides induced by natural hazard occupied 60% of all dynamics. The results manifest the importance of the proposed mechanism and its contribution to disaster monitoring and assessment.

B. Disaster Assessment

Damaged areas detected by the above regular dynamics monitoring can further be analyzed using GIS technology incorporated with hydrological, geological, and land-use information. Typhoon AERE is taken as example to demonstrate the disaster assessment.

From the geological formation point of view, the Shihmen Reservoir watershed is mostly covered with argillite and shale, which is soft and fragile particularly after earthquakes or heavy rainfall. The Chi-Chi earthquake, which occurred in September 1999, weakened the substrate material prior to Typhoon AERE, which dropped a maximum cumulative rainfall of 1600 mm within three days. Thus, the Chi-Chi earthquake may have been the hidden factor leading to so many landslides. Adopting the proposed mechanism, we detected more than 200 landslides
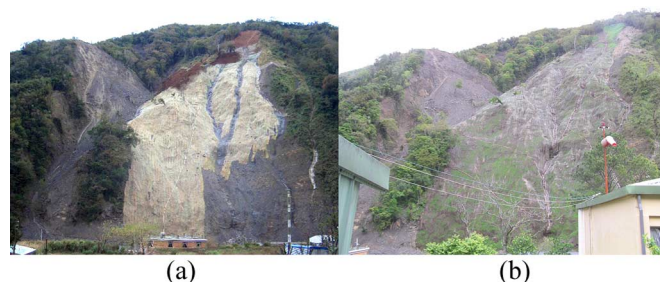

Fig. 12. Close-up photos of the Xiu-Luan landslide. (a) January 19, 2005 and (b) April 1, 2005.

with a total area of 393 ha. From the results of disaster assessment after Typhoon AERE, we found that most landslides were induced when the cumulative rainfall exceeded 800 mm. Although more than 88% of the landslides took place in natural land class, the effect of human activities still cannot be ignored.

The results using data from three major typhoons that occurred in the watershed area demonstrate the applicability and the efficiency of the established mechanism. In particular, we note that when road systems are blocked and weather conditions are unstable, on-site inspection, and aerial photo surveying are difficult to accomplish in a limited time, making the provision of a disaster assessment report almost impossible. The proposed mechanism, which uses multitemporal and multisensor satellite image, is thus an invaluable and feasible tool, provided that intensive image data are available.

C. Vegetation Recovery Monitoring

The proposed mechanism can also be applied to the monitoring of vegetation recovery. The comparisons results show that man-made reconstruction is more effective, but this is only practical when the budget is sufficient. That would be a tradeoff for reservoir managers.

REFERENCES

[1] Central Geological Survey, MOEA, "Geologic map of Taiwan, scale: 1/500 000," in *Central Geological Survey*. Taipei, Taiwan: Ministry Economic Affairs, 2000.

[2] C. S. Ho, "An introduction to the geology of Taiwan: Explanatory text of the geologic map of Taiwan," in *Central Geological Survey*. Taipei, Taiwan: Ministry Economic Affairs, 1986.

[3] *Seismic Database*, Sep. 21, 1999, Taipei, Taiwan: Central Weather Bureau. [Online]. Available: http://www.cwb.gov.tw/V5e/index.htm

[4] S. J. Dadson, N. Hovius, H. Chen, W. B. Dade, J. C. Lin, M. L. Hsu, C. W. Lin, M. J. Horng, T. C. Chen, J. Milliman, and C. P. Stark, "Earthquake-triggered increase in sediment delivery from an active mountain belt," *Geology*, vol. 32, no. 8, pp. 733–736, Aug. 2004.

[5] D. K. Keefer, "Landslides caused by earthquakes," *Geol. Soc. Amer. Bull.*, vol. 95, no. 4, pp. 406–421, 1984.

[6] D. K. Keefer, "The importance of earthquake-induced landslides to longterm slope erosion and slope-failure hazards in seismically active regions," *Geomorphology*, vol. 10, pp. 265–284, 1994.

[7] C. F. Pain and J. M. Bowler, "Denudation following the November 1970 earthquake at Madang," *Papua New Guinea: Zeitschrift für Geomorphologie*, vol. 18, pp. 91–104, 1973. Supplement.

[8] A. J. Pearce and A. J. Watson, "Effects of earthquake-induced landslides on sediment budget and transport over 50 years," *Geology*, vol. 14, pp. 52–55, 1986.

[9] A. M. Wu, "Qualification of test of ROCSAT-2 image processing system," in *Proc. 24th Asian Conf. Remote Sens.*, Busan, Korea, 2003. CD-ROM.

[10] J.-Y. Rau, L. Y. Chang, T. A. Teo, K. Hsu, J. Y. Chen, L.-C. Chen, A. J. Chen, and K. S. Chen, "An operational multi-sensor geocoded production system for earth resources satellite images," in *Proc. 5th Int. Symp. RCSGSO*, Pasadena, CA, Jul. 8–11, 2003. CD-ROM.

[11] L.-C. Chen, T. A. Teo, and J.-Y. Rau, "Fast orthorectification for satellite images using patch backprojection," in *Proc. IGARSS*, Toulouse, France, 2003.

[12] E. F. Lambin and A. H. Strahler, "Change vector analysis in multitemporal space: A tool to detect and categorize land-cover change processes using multi-temporal resolution satellite data," *Remote Sens. Environ.*, vol. 48, no. 2, pp. 231–244, May 1994.

[13] M. E. Brown, J. E. Pinzon, K. Didan, J. T. Morisette, and C. J. Tucker, "Evaluation of the consistency of long-term NDVI time series derived from AVHRR, SPOT-vegetation, SeaWiFS, MODIS, and Landsat ETM+ sensors," *IEEE Trans. Geosci. Remote Sens.*, vol. 44, no. 7, pp. 1787–1793, Jul. 2006.

[14] Z. Jiang, A. R. Huete, J. Li, and Y. Chen, "An analysis of angle-based with ratio-based vegetation indices," *IEEE Trans. Geosci. Remote Sens.*, vol. 44, no. 9, pp. 2506–2513, Sep. 2006.

[15] K. B. Kidwell, *Global vegetation index user's guide*. Washington, DC: U.S. Department of Commerce/National Oceanic and Atmospheric Administration/National Environmental Satellite Data and Information Service/National Climatic Data Center/Satellite Data Services Division, 1990.

[16] R. B. Boone, K. A. Galvin, N. M. Smith, and S. J. Lynn, "Generalizing El Niño effects upon Maasai livestock using hierarchical clusters of vegetation patterns," *Photogramm. Eng. Remote Sens.*, vol. 66, no. 6, pp. 737–744, 2000.

[17] USGS, *Landslide Types and Processes*, Jan. 2006, USG. [Online]. Available: http://pbs.usgs.gov/fs/2004/3072/

[18] *Emergency Response and Disposal Report*, Taipei, Taiwan: Ministry Interior. [Online]. Available: http://www.nfa.gov.tw/

Jiann-Yeou Rau was born in Taiwan, R.O.C, in 1964. He received the M.S.E. degree in atmospheric physics and the Ph.D. degree in civil engineering from the National Central University (NCU), Taoyuan, Taiwan, in 1988 and 2002, respectively.

He was with the Center for Space and Remote Sensing Research (CSRSR), NCU, in 1990, as an Assistant Research Scientist, where he is currently a Specialist for photogrammetry and remote sensing at CSRSR. His research activities are mostly concentrated in the domain of digital photogrammetry, land-use monitoring, cyber city modeling, image feature extraction, lidar applications, and so on.

Dr. Rau is a member of the Chinese Society of Photogrammetry and Remote Sensing and a member of Image Processing and Pattern Recognition, Taiwan.

Liang-Chien Chen was born in Taiwan, R.O.C., in 1951. He received the M.S.E. degree from the National Cheng Kung University (NCKU), Tainan, Taiwan, in 1974, and the Ph.D. degree from the University of Illinois, Urbana, in 1985.

He was with the Institute of Photogrammetry, NCKU, from 1985 to 1986. Since 1986, he has been a Professor with the Center for Space and Remote Sensing Research, National Central University, Taoyuan, Taiwan. He is in charge of the Digital Photogrammetry Laboratory and the Earth Resource Satellite Ground Receiving Station. His research activities are focused in the domain of digital photogrammetry, geometrical data processing for remotely sensed data, image feature extraction, lidar processing, and terrain analysis.

Jin-King Liu was born in Taiwan, R.O.C., in 1954. He received the M.S.C. degree in remote sensing from University College, London, U.K., and the Postgraduate Diploma in soil survey from the International Institute for Geo-Information Science and Earth Observation, The Netherlands.

Since 1977, he has been working as a Researcher of geosciences in the Industrial Technology Research Institute dedicated in the areas of geohazard research applications of remote sensing and geoinformatics.

Mr. Liu is a Councilor of the Chinese Taipei Society of Photogrammetry and Remote Sensing and National Correspondent for the International Society for Photogrammetry and Remote Sensing Commission VII.

Tong-Hsiung Wu was born in Taiwan, R.O.C., in 1949. He received the M.S.E. degree in civil engineering from the National Central University, Taoyuan, Taiwan, in 2002.

He was with the North Region Water Resource Office (NRWRO), Lung-Tan, Taoyuan, as Chief of the Protection Section, from 2001 to 2005. He is currently a Chief the Construction Section, NRWRO. His major interests are on the water resources and environmental engineering.